

# The characteristics of host lipid body biogenesis during coral-dinoflagellate endosymbiosis

Hung-Kai Chen<sup>1</sup>, Sabrina L. Rosset<sup>1</sup>, Li-Hsueh Wang<sup>1,2</sup> and Chii-Shiarng Chen<sup>1,2,3</sup>

<sup>1</sup> National Museum of Marine Biology and Aquarium, Pingtung, Taiwan

<sup>2</sup> Graduate Institute of Marine Biology, National Dong-Hwa University, Pingtung, Taiwan

<sup>3</sup> Department of Marine Biotechnology and Resources, National Sun Yat-sen University, Kaohsiung, Taiwan

## ABSTRACT

Intracellular lipid body (LB) biogenesis depends on the symbiosis between coral hosts and their Symbiodinaceae. Therefore, understanding the mechanism(s) behind LB biosynthesis in corals can potentially elucidate the drivers of cellular regulation during endosymbiosis. This study assessed LB formation in the gastrodermal tissue layer of the hermatypic coral *Euphyllia glabrescens*. Diel rhythmicity in LB size and distribution was observed; solar irradiation onset at sunrise initiated an increase in LB formation, which continued throughout the day and peaked after sunset at 18:00. The LBs migrated from the area near the mesoglea to the gastrodermal cell border near the coelenteron. Micro-LB biogenesis occurred in the endoplasmic reticulum (ER) of the host gastrodermal cells. A transcriptomic analysis of genes related to lipogenesis indicated that binding immunoglobulin protein (BiP) plays a key role in metabolic signaling pathways. The diel rhythmicity of LB biogenesis was correlated with ER-localized BiP expression. BiP expression peaked during the period with the largest increase in LB formation, thereby indicating that the chaperoning reaction of abnormal protein folding inside the host ER is likely involved in LB biosynthesis. These findings suggest that the host ER, central to LB formation, potentially facilitates the regulation of endosymbiosis between coral hosts and Symbiodinaceae.

Submitted 26 February 2021

Accepted 31 May 2021

Published 23 June 2021

Corresponding author

Chii-Shiarng Chen,

cchen@nmmba.gov.tw

Academic editor

Oren Levy

Additional Information and  
Declarations can be found on  
page 16

DOI 10.7717/peerj.11652

© Copyright

2021 Chen et al.

Distributed under

Creative Commons CC-BY 4.0

## OPEN ACCESS

**Subjects** Cell Biology, Genomics, Marine Biology, Molecular Biology, Histology

**Keywords** Coral, Diel cycle, Endoplasmic reticulum, Lipid bodies, Symbiosis

## INTRODUCTION

Endosymbiosis between coral hosts and dinoflagellates of the Symbiodinaceae family is of global importance because it serves as the energetic foundation for all coral reefs. However, systematic understanding of how this association functions at the cellular and molecular levels is lacking. A hallmark of symbiosis is the daily rhythmic lipid body (LB) formation and subsequent degradation within the gastrodermal cells of coral hosts (Chen et al., 2012). Metabolic exchange is the basis of coral–algal endosymbiosis, and we previously proposed that these LBs function as centers of this metabolic dialog (Chen et al., 2017). Therefore, LB formation is a compelling target for further research aimed at elucidating mechanisms of endosymbiosis.

LBs are ubiquitous organelles, thought to originate in specialized compartments of the smooth endoplasmic reticulum (ER) (as shown in eukaryotes, see [Wilfling et al., 2014](#)) and later bud off into the cytosol. This hypothesis is based on the location of key enzymes involved in storage lipid biosynthesis in the ER and the discovery of ER-specific proteins in LBs ([Jacquier et al., 2011](#)). According to the model proposed by [Wilfling et al. \(2014\)](#), storage lipids accumulate between sheaths of the ER membrane, and the recruitment of enzymes (involved in lipid metabolism) and accessory proteins (involved in LB budding and maturation) to the LB formation site results in LB growth. Whether mature LBs completely separate from or remain connected to the ER may vary across biological systems.

Binding immunoglobulin protein (BiP), also known as glucose-regulated protein 78 (GRP78), is an ER-specific protein and a member of the heat shock 70 protein family. Moreover, it is a central regulator of unfolded protein response (UPR) activation to ER stress ([Bertolotti et al., 2000](#)) and is associated with purified coral LBs and other lipid droplets ([Peng et al., 2011; Pratess et al., 2000; Zhang et al., 2016](#)). Furthermore, by dynamically interacting with organelles such as the Golgi apparatus, mitochondria, endosomes, lysosomes, and lipid droplets through membrane contact sites ([Cohen, Valm & Lippincott-Schwartz, 2018; Wu, Carvalho & Voeltz, 2018](#)), the ER is generally thought to be involved in not only conveying crucial cellular signals but also lipid metabolism ([Han & Kaufman, 2016](#)).

Light irradiation drives daily LB formation in corals, suggesting that photosynthetically fixed carbon is translocated to coral hosts and incorporated into the following storage lipids, constituting the cores of the LBs: triacylglycerols, sterol esters, and wax esters ([Chen et al., 2012](#)). Analyses of the lipidomic profiles of dinoflagellates, LBs, and host gastrodermal cells have suggested that hosts and endosymbionts both contribute fatty acid (FA) moieties to LB biosynthesis ([Chen et al., 2017](#)). Furthermore, a study ([Chen et al., 2012](#)) revealed that LB density peaks at sunset and returns to baseline overnight; the study also demonstrated that LBs migrate across the host gastroderm during the diel cycle, and the highest densities were observed near the mesoglea at noon and near the coelenteron at night. However, the *in situ* tissue architecture of coral tentacles used in the study was highly distorted because amputated tentacles were contracted.

Here, we tested the hypothesis that LB biosynthesis in corals occurs in the host ER. We reconfirmed this LB migration trajectory by using an improved protocol, and characterized the process of coral LB maturation using transmission electron microscopy (TEM) to analyze diel fluctuations in LB size and distribution. In addition, transcriptomic data related to UPR activation were used to elucidate the correlation among BiP, ER, and lipogenesis throughout the diel cycle. Complementary to the transcriptomic-level analysis, LB biosynthesis in corals was found to occur in the host ER when the abundance of the ER marker protein BiP in isolated LBs was measured. Understanding intracellular LB formation and maturation processes in corals can help to elucidate the mechanisms behind coral–algae endosymbiosis; such information could make tangible contributions to coral lipidomics in general, and more specifically, can be applied to research geared toward understanding and mitigating coral bleaching (i.e., the breakdown of symbiosis).

## MATERIALS & METHODS

### Coral husbandry

Corals (*Euphyllia glabrescens*) were collected from a reef at the inlet of the Third Nuclear Power Plant in Nanwan Bay, Taiwan ( $21^{\circ}57.376'N$ ,  $120^{\circ}45.291'E$ ) in 2012. Coral collection was approved by the Kenting National Park Management Office. Ten~ twelve colonies were cultured over eight years in each 4-ton tanks with flow-through seawater (exchange rate of  $\sim 80L/h$ ) in the husbandry center of the National Museum of Marine Biology and Aquarium (NMMBA). Twenty-four colonies for experiments were maintained under an ambient diel cycle with natural sunlight, and temperature was maintained at  $26.5 \pm 1^{\circ}C$  using a microprocessor-controlled cooler (First FC-45, Aquatech, Kaohsiung, Taiwan). Light intensity and water temperature were continuously recorded using a HOBO Pendant® logger placed near the colonies in each tank (UA-002; Onset, Pocasset, MA, USA).

### Analysis of *in situ* LB distribution

Tentacle samples were collected at the following nine times during one diel cycle: 06:00 (sunrise), 9:00, 12:00 (noon), 15:00, 18:30 (sunset), 21:00, 00:00 (midnight), 03:00, and 05:00. Tentacles were collected from three distinct colonies ( $n = 3$  tentacles/colony) at each time point. A single polyp was targeted only once to avoid sampling-induced stress. For accurate analysis of LBs, preserving the natural tissue architecture of the expanded tentacle was critical. Sampling the tentacle without using a capillary clip resulted in a sectioned gastroderm exhibiting multiple layers of cells containing endosymbionts (Fig. 1A). We circumvented this limitation by successfully preserving the tissue architecture of the naturally expanded tentacle with a clamping technique marked using solid arrows in Figs. 1B and 1C. To verify the effectiveness of this technique, architectural differences in the gastrodermal tissue of extended and contracted tentacles were assessed by staining LBs with osmium tetroxide, cryosectioning fixed specimens, and imaging sections by using differential interference contrast microscopy (Figs. 1A & 1D) as described by [Chen et al. \(2012\)](#). This technique allowed the gastroderm to consist of a single cell layer (Fig. 1D).

### Ultrastructure analysis through Transmission Electron Microscope

Clamped tentacles were amputated using micro scissors and immediately fixed with 2.5% glutaraldehyde and 2% paraformaldehyde in 100 mM sodium phosphate containing 5% sucrose (pH 7.3) for 2.5 h at  $4^{\circ}C$  then washed with 100 mM sodium phosphate at  $4^{\circ}C$ . Specimens were post fixed in 1% osmium tetroxide in 50 mM sodium phosphate (pH 7.3) for 1 h at  $4^{\circ}C$ . Samples and data were then proceeded and analyzed according to previously methods by [Chen et al. \(2012\)](#). Individual LB sizes were determined by measuring their maximum diameter ( $\mu m$ ), and LBs were categorized into three size classes (micro-LBs:  $<1 \mu m$ ; mid-LBs:  $1-3 \mu m$ ; large-LBs:  $>3 \mu m$ ) and two distribution categories (near the mesoglea or near the coelenteron) by using Metamorph 6.3 (Molecular Devices).

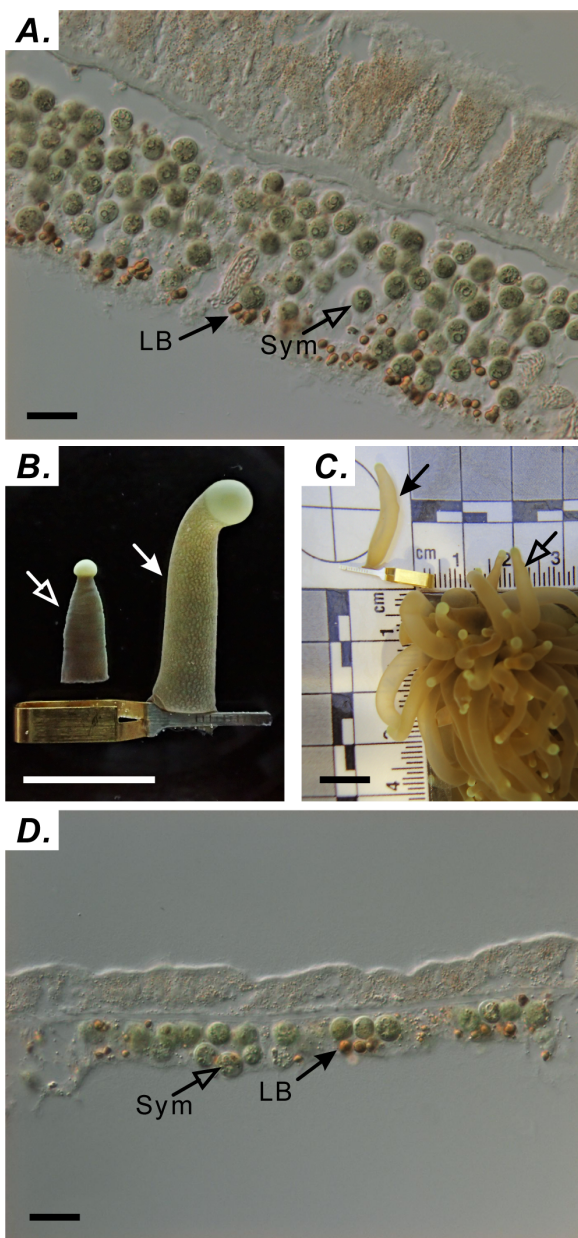


**Figure 1** Using capillary clips to fix tentacle-tissue architecture. (A) Distribution of symbionts (Sym) and lipid bodies (LBs) in tentacles without capillary-clip fixation (scale = 10  $\mu$ m). (B) Tentacles processed with (right) and without (left) the capillary clip (right; scale = one cm). (C) Comparison of tentacles with the capillary clip (solid arrow) with normal tentacle of *Euphyllia glabrescens* coral (open arrow; scale = one cm). (D) Distribution of Sym and LBs in tentacles with capillary-clip fixation (scale = 10  $\mu$ m).

Full-size DOI: 10.7717/peerj.11652/fig-1

### Transcriptomic analysis of ER genes related to LB lipogenesis Tentacle collection and RNA extraction

Tentacles (stretched to a length of ~3 cm) were amputated from polyps of *E. glabrescens* colonies at approximately sunrise (06:00), noon (12:00), sunset (18:00), and midnight (00:00) using curved surgical scissors. The tentacles were then washed twice with filtered

seawater (FSW), frozen in liquid nitrogen, and stored at  $-80^{\circ}\text{C}$ . De novo transcriptome sequencing (RNA-Seq) using Illumina technology was performed by Welgene Biotech (Taipei, Taiwan). Purified RNA was quantified at 260 nm ( $\text{OD}_{600}$ ) by using an ND-1000 spectrophotometer (Nanodrop Technology, Wilmington, DE, USA) and analyzed using a Bioanalyzer 2100 (Agilent Technologies, USA) with an RNA 6000 LabChip kit (Agilent Technologies, USA). All procedures were performed in accordance with manufacturer protocols.

### ***Sequencing and transcriptome assembly***

Libraries of all samples were created using the SureSelect Strand-Specific RNA Library Prep kit for 150 PE bp sequencing on the Solexa platform. Sequencing was performed using the TruSeq SBS Kit. Raw sequences were obtained using the Illumina Pipeline software bcl2fastq v2.0, and we expected to generate 2 Gb per sample. Trimmomatics was then used to generate qualified reads by trimming or removing low-quality bases or reads ( $\text{QV} \geq 20$ ) ([Bolger, Lohse & Usadel, 2014](#)). All qualified 150 PE reads were assembled using the de novo assembly program Trinity ([Grabherr et al., 2011](#)). After Trinity assembling, CD-HIT-EST was used to remove contig sequence redundancy ([Fu et al., 2012](#)). Unigene names were assigned by the partitioning algorithm in the khmer software package ([Crusoe et al., 2015](#)). Estimations of unigene abundance were calculated using Cufflinks.

### ***Functional annotation of assembled unigenes***

Unigenes in the transcriptome assembly were searched against the National Center for Biotechnology Information nonredundant protein (nr), Gene Ontology (GO), and Kyoto Encyclopedia of Genes and Genomes (KEGG) Pathway databases by using the high-efficiency alignment algorithm RAPSearch2 with a cutoff  $E$  value  $\leq -3$  ([Zhao, Tang & Ye, 2011](#)). The top alignment hits were used to predict the sequence orientations, GO accessions, and related KEGG Pathways of the unigenes. KEGG and GO functional classification for genes related to lipogenesis and LB formation was used to understand the distribution of gene functions in the coral host at the macro level. We used the fold change to assess the distributions and variations of genes related to LB lipogenesis for four sampling times.

### ***Expression analysis of ER genes related to lipogenesis***

Qualified 150 PE reads were mapped using the short-read alignment software Bowtie2 ([Langmead & Salzberg, 2012](#)). After mapping, the expression estimation of each gene was quantified using Cufflinks ([Trapnell et al., 2012](#)). Gene expression levels were calculated as fragments per kilobase of transcript per million mapped reads (FPKM). Furthermore, gene expression levels at different diel-cycle times were calculated as relative expression values of each sampling time. We adopted  $\log_2$  (FPKM ratio) as the fold change of gene expression, that is, sunrise =  $\log_2(\text{FPKM}_{\text{sunrise}}/\text{midnight})$ , noon =  $\log_2(\text{FPKM}_{\text{noon}}/\text{sunrise})$ , sunset =  $\log_2(\text{FPKM}_{\text{sunset}}/\text{noon})$  and midnight =  $\log_2(\text{FPKM}_{\text{midnight}}/\text{sunset})$ . FPKM and bioinformatic calculations were also performed by Welgene Biotech (Taipei, Taiwan). JMP v.10 (SAS Institute Inc., Cary, NC, USA) was used to translate the fold changes ( $\log_2$  FPKM) of gene expression and the density distribution of gene expression profiles.

## Diel expression pattern of BiP in host cells and purified LBs

### Tentacle collection and LB isolation

Tentacles were sampled at six time points during the diel cycle: 06:00, 12:00, 15:00, 18:00, 21:00, and 00:00. For a given sampling time, a total of 80 tentacles were collected (pooled from multiple colonies). This sampling strategy was repeated for three distinct diel cycles ( $n = 3$  different sampling days). After rinsing tentacles with FSW, tentacle tips were removed to prevent interference from nematocysts. The gastroderm was then separated from the epiderm through incubation with 3% *N*-acetylcysteine (pH 8.2, prepared in artificial seawater) for 1 h at room temperature (RT) (Peng et al., 2008). LBs samples and data were then proceeded and analyzed as previously described (Chen et al., 2012; Chen et al., 2017; Peng et al., 2011).

### Fluorescence staining of purified LB

Lipid-specific fluorescent dye BODIPY 493/503 (Thermo Fisher Scientific) was prepared in ethanol as a 3.82 mM (1 mg/mL) stock. Each specimen was stained for 20 min with a working solution that was a 1:100 dilution of the stock (Gocze & Freeman, 1994). A fluorescein isothiocyanate (FITC) filter was used for green fluorescence imaging. The ER-specific staining dye ER-Tracker Blue-White DPX (Thermo Fisher Scientific) was prepared in a 1 mM dimethyl sulfoxide stock. LB specimens were stained for 1 h using a working solution that was a 1:250 dilution of the stock (Diwu et al., 1997). A 4',6-diamidino-2-phenylindole filter and FITC filter were used for blue and green fluorescence, respectively.

### Western blotting of BiP

Host gastrodermal cells were lysed, and LBs were delipidated in accordance with the procedures described by Mastro & Hall (1999) by adding a delipidation solution (tributyl phosphate: acetone: methanol, 1:12:1 v/v/v) to the collected fractions at a 14:1 v/v ratio on ice. This was followed by incubation at  $-20^{\circ}\text{C}$  overnight. Preprocessing of protein samples for SDS-PAGE analysis were proceeded as previously described in Peng et al. (2011).

Twenty micrograms of each protein sample were subjected to 12% SDS-PAGE then blotted onto polyvinylidene fluoride membranes (Immobilon-PSQ 0.45 mm; Millipore, Germany). The membranes were incubated in 5% skim milk in tris-buffered saline, 0.1% Tween-20 (TBST), 100 mM Tris (pH 7.6), and 150 mM NaCl at RT for 1 h. Incubation was then performed with rabbit anti-GRP78/BiP (ET-21) antibody (1:2000 dilution; cat. no G9043 Sigma-Aldrich) and preimmune serum antibodies (1:5000 dilution) in TBST buffer at  $4^{\circ}\text{C}$  overnight. The membranes were then washed five times with TBST buffer for 10 min each, incubated with horseradish-peroxidase-conjugated goat anti-rabbit IgG antibodies (Millipore) in TBST buffer (1:5000 dilution), washed with TBST buffer, and visualized using a SuperSignal West Pico chemiluminescent substrate kit (cat. no 34080, Thermo Fisher Scientific) in accordance with manufacturer recommendations. Experiments were repeated in triplicate, and ImageJ was used to quantify band intensity for protein expression levels (Schneider, Rasband & Eliceiri, 2012). Relative BiP expression in the LB (or host) fraction was calculated as follows: the ratio of BiP in LB (or host) = the

intensity quantification value in the LB (or host) fraction/the total intensity quantification value in the LB and host.

### Statistical analysis

Data were analyzed using SPSS (version 14.0; SPSS Inc., Armonk, NY, USA). One-way analyses of variance and Tukey pairwise comparisons were conducted to determine the effect of sampling time on LB density, size, location, and gene and protein expression, and results were considered statistically significant when  $p$  was  $<0.05$ . Values are presented as means  $\pm$  SDs.

## RESULTS

### Ultrastructural and morphological characteristics of host LBs in the gastrodermis

Similar to the biogenesis of lipid droplets in other eukaryotic cells, that of LBs in coral–Symbiodiniaceae endosymbiosis has several unique morphological characteristics. We find multiple lines of evidence suggesting that lipid droplets are derived from the ER. First, coral host LBs were in close spatial proximity to mitochondria (Fig. 2), endoplasmic reticulum (ER, Fig. 2A), and Golgi apparatus (Fig. 2D and 2G), which exhibit high electron density upon transmission electron microscopy (TEM) examination. Our *in situ* morphology of coral host LBs revealed that they originate in the ER (Fig. 2A) and are surrounded by the ER (Fig. 2B). Figures 2B and 2C illustrates that micro-LBs and some mid-LBs accumulated in the coral host ER and then migrated and fused together. LBs formed a single globule with few inclusion bodies (Figs. 2C–2F) and had dense Golgi spots (Figs. 2D and 2G). When fusion occurred, numerous granules with high-electron density (Figs. 2E, 2F, 2H and 2I) appeared within the mid-LBs as they fused with micro-LBs, (Figs. 2E and 2H), and when mid-LB fused with large-LB (Figs. 2F and 2I). Finally, large-LBs continued to integrate into larger LBs.

### Diel pattern of LB size and distribution

To assess the spatiotemporal dynamics of coral LBs during the diel cycle, gastrodermal LBs were analyzed using TEM for three sizes (i.e., micro-LBs:  $<1\ \mu\text{m}$ ; mid-LBs:  $1\text{--}3\ \mu\text{m}$ ; large-LBs:  $>3\ \mu\text{m}$ ) and two distributions near the mesoglea or coelenteron within the gastroderm (Fig. 3A). Total LBs started to increase at sunrise and gradually increased during the day, reaching maximum density at sunset (Fig. 3B).

Micro-LBs comprised the largest portion of LBs throughout the diel cycle (Fig. 3C; Table S1). A significantly larger portion of micro-LBs were located near the mesoglea (approximately 40–80%) and they increased moderately throughout the diel cycle (Fig. 3C; Table S1; light period:  $37.2 \pm 2.9\%$  to  $44.3 \pm 3.8\%$ ; dark period:  $40.1 \pm 3.4\%$  to  $53.3 \pm 2.8\%$ ). The percentage of micro-LBs near the coelenteron gradually decreased from  $22.3 \pm 1.7\%$  at sunrise to  $10.0 \pm 3.1\%$  at sunset (Fig. 3C; Table S1) and increased overnight to  $13.8 \pm 1.6\%$  at 21:00 and  $20.3 \pm 4.2\%$  at 05:00. The number of mid- and large-LBs near the mesoglea remained relatively low ( $0.7 \pm 0.3\%$  and  $13.5 \pm 4.4\%$ , respectively; Fig. 3C; Table S1) and nonsignificantly different during the diel cycle (mid-:  $p = 0.45$ ; large-:  $p = 0.11$ ).

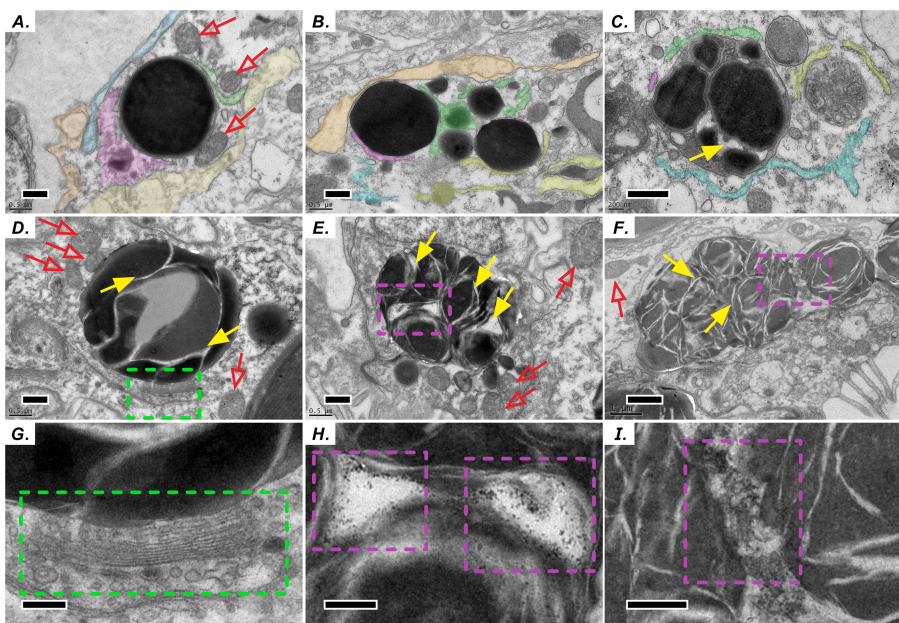


**Figure 2** Diel biosynthesis of host LBs in the gastroderm. (A) LBs from the endoplasmic reticulum (ER, see colored areas, and different colours represent some fragments of ER) surrounded by mitochondria (red arrows; scale = 0.5  $\mu\text{m}$ ). (B) LBs enveloped by ER (solid red arrows; scale = 0.5  $\mu\text{m}$ ). (C) Fused LBs (scale = 0.5  $\mu\text{m}$ ). (D) LBs forming a single globule with several inclusion bodies (scale = 0.5  $\mu\text{m}$ ). (E) Single-globule LB continuing to fuse other micro-LBs with inclusion bodies (see solid yellow arrows, scale = 0.5  $\mu\text{m}$ ). High-electron density granules appeared within LBs. (F) Two mid-LBs fused together, and high-electron-density granules (see purple dashed frame) appeared within large-LBs (scale = 1  $\mu\text{m}$ ). (G) Enlargement of the red dashed frame in (D) displaying LB fusing near a Golgi apparatus and vesicles (see green dashed frame, scale = 0.2  $\mu\text{m}$ ). (H) Enlargement of the red dashed frame in (E). High-electron-density granules are visible between two fusing LBs (scale = 0.2  $\mu\text{m}$ ). (I) Enlargement of the red dashed frame in (F) (scale = 0.2  $\mu\text{m}$ ).

Full-size DOI: 10.7717/peerj.11652/fig-2

However, LB populations close to the coelenteron exhibited significant diel fluctuations (mid- and large-:  $p < 0.05$ ). The percentage of these larger LBs increased during the light period and returned to baseline levels overnight (Fig. 3C). The peak in relative abundance for mid- and large-LBs near the coelenteron occurred at 18:30 ( $23.3 \pm 1.1\%$ ) and 21:00 ( $19.3 \pm 1.7\%$ ), respectively.

### Transcriptomic analysis of UPR activation/ER stress genes related to lipogenesis

In response to ER stress, a signal transduction pathway known as UPR is activated, and it may affect the metabolic process of de novo lipid biosynthesis. We analyzed the transcriptome of the coral *Euphyllia glabrescens* and focused on unigenes and pathways related to LB metabolism. LB lipogenesis occurs primarily in host cells, where metabolic signals regulate the expression of key enzymes in lipogenic pathways (Fig. 4A, modified from previous models; (Morris *et al.*, 1997; Zheng, Zhang & Zhang, 2010; Basseri & Austin, 2012)). Specifically, as a monitor of UPR activation/ER stress, the ER chaperone and signaling regulator GRP78/BiP exhibited a fourfold increase in expression at noon. Nearly

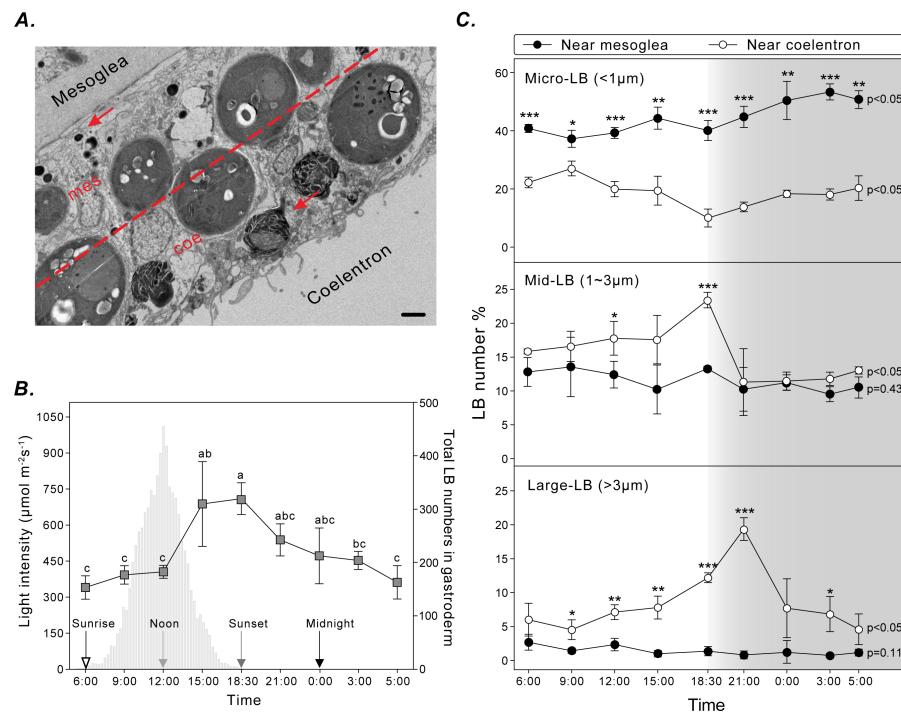


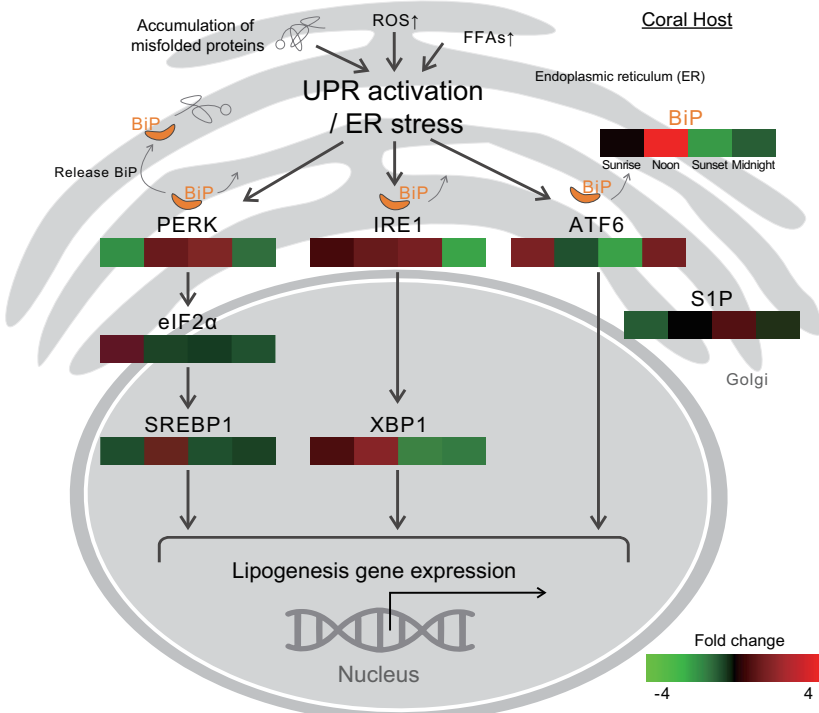
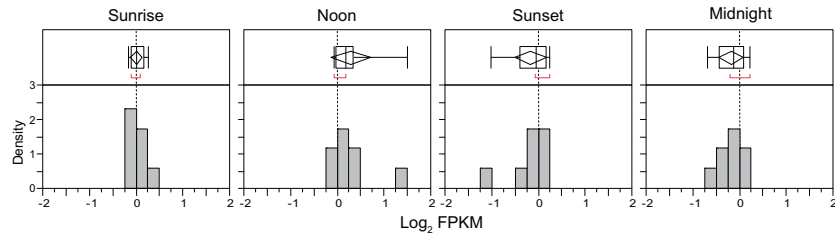
**Figure 3 LB size and distribution during the diel cycle.** (A) LB distribution was examined by calculating the number of LBs (red arrow) in two gastrodermal regions: the region near the mesoglea (mes) and the region near the coelenteron (coe; scale = 2  $\mu\text{m}$ ). (B) Photosynthetically active radiation and total LBs during a typical diel cycle. (C) Changes in size and distribution of LBs during the diel cycle. Data are presented as mean  $\pm$  standard deviation ( $n = 3$ ), \*  $p < 0.05$ , \*\*  $p < 0.01$ , \*\*\*  $p < 0.001$  (mesoglea vs. coelenteron; Table S1).

Full-size DOI: [10.7717/peerj.11652/fig-3](https://doi.org/10.7717/peerj.11652/fig-3)

simultaneously, the two sensor proteins protein kinase R-like ER kinase (PERK) and inositol-requiring enzyme 1 (IRE1), which induce various pathways and drive lipid biosynthesis, exhibited near a two-fold increase in expression. IRE1 expression started to increase at sunrise and could reach a two-fold change in transcription factor X-box binding protein 1 (XBP1) expression by noon. The eukaryotic translation initiation factor 2 subunit 1 (eIF2  $\alpha$ ) expression started to increase twofold change at sunrise. Transcription factor sterol regulatory element-binding protein 1 (SREBP1) activated by PERK also had increased expression at noon. The activating transcription factor 6 (ATF6) sensor protein was activated after midnight, whereas membrane-bound transcription factor site-1 protease (S1P) exhibited increased expression at sunset. Figure 4B presents a box plot of the distributions and outliers of gene expression for UPR activation/ER stress genes related to LB lipogenesis. Genes including BiP, PERK, eIF2 $\alpha$ , SREBP1, IRE1, XBP1, ATF6, and S1P were upregulated starting at sunrise and downregulated from sunset to midnight.

### Diel fluctuations of ER marker BiP locations

Figure 5A illustrates the successful fluorescence staining of purified LBs with lipid marker BODIPY 493/503 and ER-tracker Blue-White dye. The LBs contained neutral lipids and were enclosed in an ER membrane. The aforementioned *in situ* morphological findings

**A. Lipogenesis of UPR activation / ER stress****B. Distributions of gene expression values**

**Figure 4** Transcriptomic analysis of ER stress genes related to LB lipogenesis. (A) ER stress activates the ER stress transducers PERK (left), IRE1 (center), and ATF6 (right) in the ER membrane. The orientation of the colored box corresponds to time points (i.e., sunrise, noon, sunset, and midnight) during the diel cycle. The color scale represents gene fold changes ( $\log_2$  fragments per kilobase of transcript per million mapped reads) of gene expression (i.e., a red box represents a fourfold increase, and a green box represents a fourfold decrease). (B) Box plot of the distribution and outliers of gene expression levels for UPR activation/ER stress genes related to lipogenesis at sunrise, noon, sunset, and midnight.

Full-size DOI: 10.7717/peerj.11652/fig-4

also supported this finding (Fig. 2). BiP was selected to be an ER-specific marker protein to assess the functional association of coral gastrodermal LBs with the host ER. BiP expression was detected only in the coral host and purified LBs but not in endosymbionts (Fig. 5B). Furthermore, the 78-kDa BiP doublet was present in the purified LBs, indicating the close association of BiP with LBs. The two bands of BiPs in the host and purified LBs (Fig. 5B) were removed and analyzed using mass spectrometry (Fig. S1). The upper band in both LBs and the host was identified as a 78-kDa glucose-regulated protein (GRP78/BiP), and the lower band in the host fraction was identified as a 73-kDa heat shock protein (HSP70).

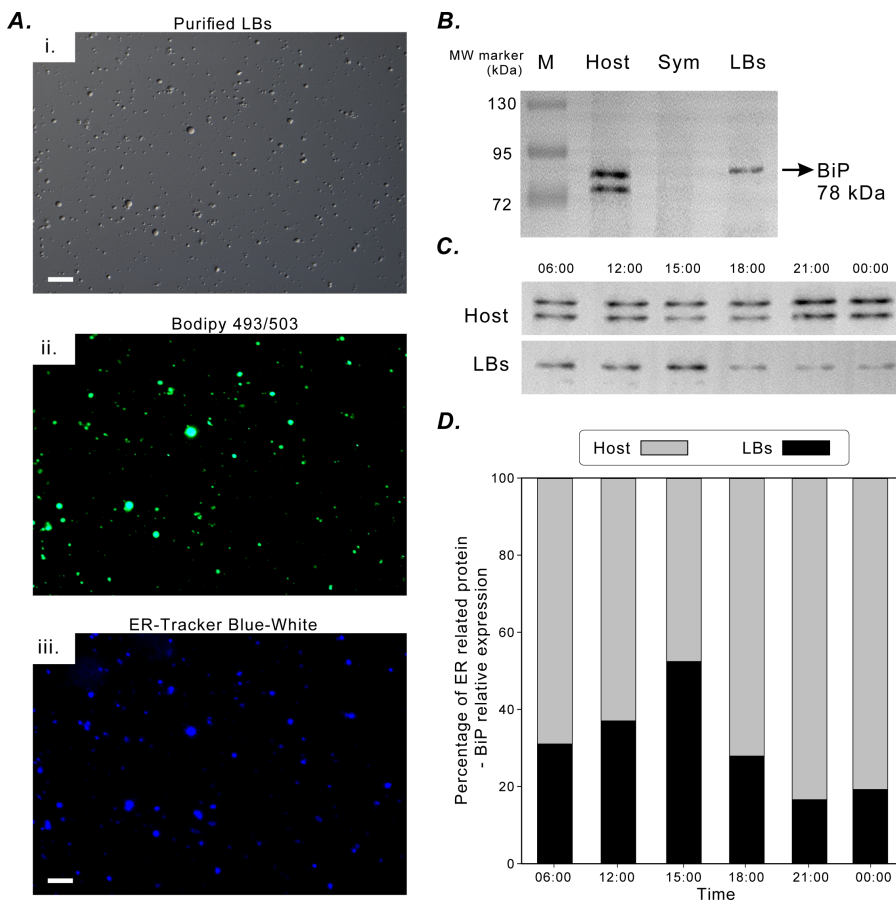


**Figure 5** BiP expression during the diel cycle. (A) [i] Lipid Bodies (LBs) purified from gastrodermal cells under differential interference contrast microscopy. [ii] LBs stained with the neutral lipid marker Bodipy 493/503. [iii] LBs stained with endoplasmic reticulum (ER)-tracker Blue-White dye, which indicated that LBs were enclosed in an ER membrane (scale = 10  $\mu$ m). See Fig. S4 for different merging images. (B) BiP expression in the coral host (Host), dinoflagellate endosymbionts (Sym), and isolated LBs after Western blotting with the rabbit anti-BiP antibody. (C) BiP expression in the coral host (Host) and isolated LBs (LBs) during the diel cycle after Western blotting. (D) Further quantification and plotting of blots. See Figs. S2, S3 and Table S3 for the full-length blots and percentages of ER-related BiP expression in the host and LB fractions.

Full-size DOI: 10.7717/peerj.11652/fig-5

BiP expression during the diel cycle was assessed through Western blotting (Fig. 5C) and then quantified (Fig. 5D). To understand the relative ratios of BiP involved in LB lipogenesis of the total host fraction, the diel fluctuations in the relative concentration of BiP associated with purified LBs were assessed and compared with those of the remaining host fraction (Fig. 5D). The relative expression of BiP associated with LBs increased significantly at 15:00 and decreased at 18:00 (Fig. 5D). In addition, BiP abundance in the host fraction was significantly higher at night and peaked at 21:00. Thus, BiP exhibited distinct temporal fluctuation patterns in the LB and host fractions.

## DISCUSSION

### Cytological characteristics of LB formation reveal LB origin

We successfully preserved the gastroderm consisting of a single layer of cells (Fig. 1). LBs move to self-assemble and fuse with each other (Boström *et al.*, 2005). This is consistent with our observations that smaller LBs fuse to form larger LBs, resulting in irregularly shaped large LBs (Figs. 2B and 2C). The fusion of several smaller lipid droplets to larger lipid droplets also contributes to lipid droplet growth (Guo *et al.*, 2008; Cheng, Fujita & Ohsaki, 2009). The LBs were in close spatial proximity to mitochondria, ER, and Golgi apparatus. Originating from the ER, lipid droplets can associate with most other cellular organelles through membrane contact sites (Jacquier *et al.*, 2011; Peng *et al.*, 2011; Olzmann & Carvalho, 2019). LB mobility was also attributed to the dynamic interactions of LBs with other organelles, including mitochondria (Figs. 2A, 2D, 2E and 2F), ER (Fig. 2A, Fig. 2B and Fig. 2C), the Golgi apparatus (Fig. 2D and 2G), peroxisomes, endosomes, and lysosomes (Herms *et al.*, 2015; Gao & Goodman, 2015; Crossland, Barnes & Borowitzka, 1980; Hayes & Goreau, 1977; Vandermeulen, 1974). Therefore, LBs may play a role in the intracellular trafficking of lipids as well as proteins and other molecules between organelles. Moreover, LBs may migrate within host gastrodermal cells toward intracellular sites of lipid utilization and catabolism. Importantly, LBs biogenesis and degradation, as well as their interactions with other organelles, are tightly coupled to cellular metabolism and facilitate the coordination and communication between different organelles and act as vital hubs of cellular metabolism (Olzmann & Carvalho, 2019). In many cells, lipid droplets undergo active motion, typically along microtubules. This motion has been proposed to aid growth and breakdown of droplets, to allow net transfer of nutrients from sites of synthesis to sites of need and to deliver proteins and lipophilic signals (Pol *et al.*, 2004; Welte, 2009). Thus, nascent LB globule biogenesis likely occurs near the mesoglea. As LBs grow and mature, they migrate across gastrodermal cells and fuse to form large LBs adjacent to the coelenteron.

The time-dependent LB relocation may occur inside a single gastrodermal cell during their biogenesis which ultimately manifests as a redistribution of LBs across the gastrodermal tissue layer. LBs move along microtubules and relocate within the cytoplasm (Welte, 2009). A proteomic investigation indicated that cytoskeletal proteins and proteins involved in intracellular trafficking were associated with coral LBs (Peng *et al.*, 2011). The mechanism by which LB populations migrate across the gastroderm to cause this redistribution remains unknown. By correlating LB size and location throughout the diel cycle in naturally expanded tentacle specimens, a study validated the proposed redistribution of LBs from the mesoglea to the coelenteron (Chen *et al.*, 2012). Our data further demonstrated that micro- and mid-sized LBs fuse to form large LBs near the coelenteron. In particular, micro-LBs were the most abundant near the mesoglea, whereas mid- and large-sized LBs increased in abundance near the coelenteron during the light period (Fig. 3). This finding was consistent with a previous study suggesting that LBs migrate across the gastroderm during the diel cycle (Chen *et al.*, 2012).

## Transcriptional variation of BiP is correlated with LB lipogenesis

Ultrastructural morphology studies have revealed that lipid droplets are closely associated with the ER membrane (Fig. 2), and proteomic studies of lipid droplets isolated from various cell lines have revealed numerous ER proteins (Chen et al., 2012; Peng et al., 2011; Liu et al., 2004; Brasaemle et al., 2004; Wan et al., 2007). The ER is the main site of the synthesis of lipids that constitute most of the lipid components of all biological membranes, and the ER is highly sensitive to changes in intracellular homeostasis and extracellular stimuli. During the perturbation of ER homeostasis, referred to as ER stress, UPR is activated when misfolded proteins accumulate, when reactive oxygen species (ROS) are produced, or when the accumulation of FAs resulting from lipolysis alter ER membrane lipids (Volmer & Ron, 2015; Walter & Ron, 2011; Chitruju et al., 2017). We demonstrated that the increase in BiP gene expression from sunrise to noon (Fig. 4) may reflect a localized increase in BiP in daytime within the ER microdomain involved in LB formation (Fig. 5). BiP is the primary regulator of the UPR and is upregulated in response to ER stress (Bertolotti et al., 2000; Morris et al., 1997). Furthermore, PERK and IRE1 cascade facilitates LB formation and possibly lipogenesis, and the ATF6 branch enhances phospholipid biosynthesis (Zheng, Zhang & Zhang, 2010; Basseri & Austin, 2012; Zha & Zhou, 2012). Our transcriptomic variation results (Fig. 4B) were also consistent with those of previous studies, which indicated a general increase in total lipids, FA concentration, and density in LBs during the light period followed by a decrease at night (Chen et al., 2012; Chen et al., 2017).

In addition to its core function in lipid formation, the diel cycle may provide a mechanism for managing daily oxidative stress induced by photosynthesizing Symbiodinaceae in coral host tissue (Levy et al., 2006). In addition to ROS production in the ER resulting from oxidative protein folding, this could overwhelm ER homeostasis and induce daily ER stress response (Malhotra & Kaufman, 2007; Levy et al., 2011; Oakley et al., 2017). LB formation may play a role in alleviating ER stress by sequestering unfolded proteins and transiently storing them for degradation (Ploegh, 2007). This has been supported by the observations of increased LB biogenesis induced by ER stress (Fei et al., 2009; Lee et al., 2012), but this functional link remains uncertain (To et al., 2017).

## Translational fluctuations of BiP revealed LB origins

After analyzing diel transcriptional variations and the transcriptomic pathway, we selected the ER marker BiP associated with LBs to elucidate the connection among LB formation, the ER, and the diel cycle. We observed an increase in the relative concentration of BiP associated with LBs in midafternoon (Fig. 5). However, BiP expression in the host fraction continued to increase at night (21:00). The increase in the apparent relative abundance of BiP may be due to an increase in either ER network volume or localized BiP concentration in response to upregulated BiP expression. Our current data cannot be used to distinguish one cause from the other. Nevertheless, the consistent association of BiP with LBs throughout the diel cycle and the diel patterns in BiP concentrations between the LB and host fractions demonstrated that LBs are closely associated with a specialized domain of the host ER. The peak in LB-associated BiP was associated with an increase in the total volume of LBs (Fig. 5), thereby supporting the involvement of ER expansion in LB biosynthesis. Moreover,

the nocturnal increase in host ER BiP but not in LB formation may indicate ER expansion at night. The ER is a dynamic organelle, and its tubular network can expand to meet the demands of ER-based processes, including protein folding, modification, and secretion; lipid metabolism; and calcium homeostasis (*Federovitch, Ron & Hampton, 2005*).

A persisting question in LB research is whether LBs ever truly detach from the ER (*Mishra et al., 2016*). This is particularly relevant considering the substantial migration and fusion of LBs in the coral gastroderm. After the peak in LB-associated BiP occurred in the midafternoon, the relative BiP concentration decreased at sunset (*Fig. 5D*). However, total LB volume reaches its highest concentration at sunset (*Chen et al., 2012; Chen et al., 2017; Peng et al., 2011*). Therefore, larger LBs that dominate at sunset likely detach from the ER or are at least less closely associated with the ER. The continuity of the ER membrane with the LB surface may be maintained permanently with stalk-like projections of the ER membrane that allow for the continued lipid and protein trafficking between the organelles (*Jacquier et al., 2011; Zehmer et al., 2009*). Moreover, the dynamic fluctuation of BiP expression between the coral host and LBs rules out the possibility that BiP within the LBs was merely an impurity collected in the isolation process. Rather, our findings suggested that coral gastrodermal LBs are functionally connected to a specialized domain of the host ER.

### Dynamic schematic model of LB formation

Coral gastrodermal LBs are highly dynamic organelles, and LB formation is highly associated with coral host ER. Imaging analyses of ultrastructural morphological characteristics and the Western blotting of BiP–ER marker protein distribution supported the model of LB formation (*Fig. 6*). We developed this model of ER involvement in LB biogenesis to illustrate the distribution of BiP expression between a coral host and LBs (*Fig. 6A*), resulting in dynamic fluctuations in BiP expression (*Fig. 5*). Furthermore, we proposed a six-stage process of LB formation and maturation (*Fig. 6B*). First, micro-LBs bud from the ER surrounded by mitochondria (*Fig. 6B* [i]). Subsequently, more micro-LBs gather and are surrounded by ER sheaths (*Fig. 6B* [ii]). In the third stage, micro-LBs fuse into larger LBs with different lipid compositions (*Fig. 6B* [iii]). This might result in different colors in TEM image analysis. During the diel cycle, LB growth and fusion result in mid-LBs. At the same time, a large population of micro-LBs is maintained (*Fig. 6B* [iv]); this occurs with dense Golgi spots in particular. Mid-LBs continue to fuse to form large-sized LBs (>6  $\mu\text{m}$ ). When fusion occurs, numerous “dots” form on vesicles in between the LBs, as illustrated in *Fig. 6* [v]. Finally, the large-LBs fuse to form mature LBs, as presented in *Fig. 6* [vi].

LB size must be strictly regulated to balance lipid storage and mobilization in response to energetic demand (*Yang et al., 2012*). In response to excess lipid molecules, a cell can increase either the number of LBs or the size of existing LBs. Changes to LB size alter the LB volume-to-surface-area ratio, which affects the rate of LB catabolism. The formation of large LBs as observed in the coral gastroderm (*Fig. 3C*) is the most efficient form of lipid storage (*Yang et al., 2012*). Moreover, micro-LBs potentially function to meet immediate energetic demands because of the rapid availability of lipids for catabolism and oxidation (*Ariotti et al., 2012*). Therefore, heterogeneity in gastrodermal LBs may reflect

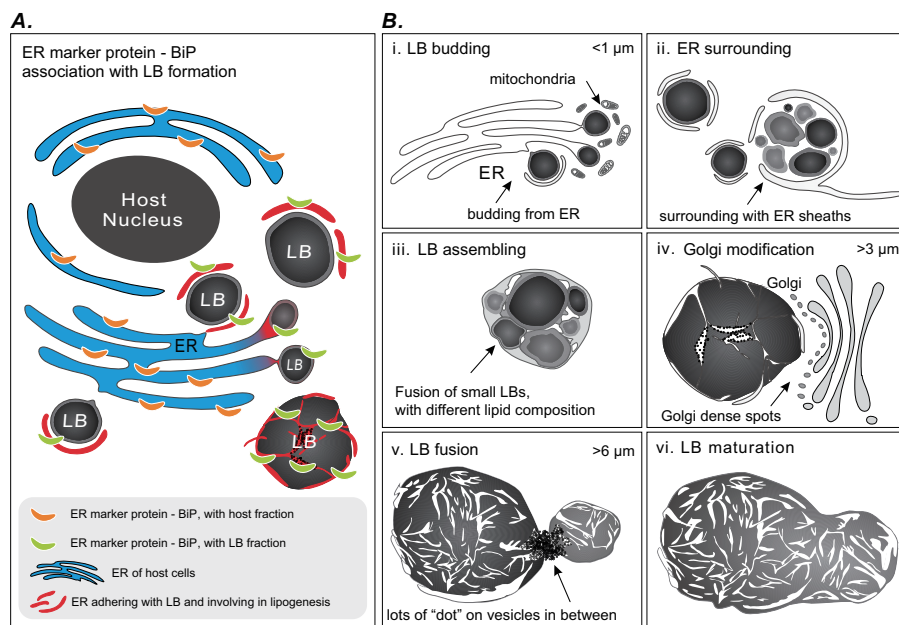


**Figure 6** Schematic summary of LB formation in coral–Symbiodinaceae endosymbiosis. (A) Proposed model of endoplasmic reticulum (ER) involvement in LB biogenesis resulting in the BiP expression distribution between coral host and LBs. (B) LB formation and maturation. [i] LB budding. [ii] ER surrounding. [iii] LB assembling. [iv] Golgi modification. [v] LB fusion. [vi] LB maturation.

Full-size DOI: 10.7717/peerj.11652/fig-6

diversity in LB functions ([Zhang et al., 2016](#)). The overnight disappearance of large LBs was hypothesized to occur because of nocturnal lipid catabolism and utilization ([Chen et al., 2012](#)), however, the underlying mechanism is not clear.

## CONCLUSIONS

Unique diel rhythmicity in LB biosynthesis, growth, and maturation was observed in coral gastrodermal cells, and these processes may play a key role in regulating coral–Symbiodinaceae endosymbiosis ([Chen et al., 2012](#); [Chen et al., 2017](#); [Peng et al., 2011](#)). The daily cycle of LB formation, maturation, and degradation is a cellular process underpinning stable coral–Symbiodinaceae endosymbiosis ([Chen et al., 2012](#); [Peng et al., 2011](#)). By demonstrating that LB biogenesis is localized in the host ER, this study provided new insight into the mechanism of metabolite integration within this symbiosis. LBs are composed of FA moieties with both host and symbiont origins ([Chen et al., 2017](#)). Therefore, lipid molecules translocated from the symbiont to the host may be transported to the host ER where they enter storage lipid biosynthetic pathways in the host and become integrated into LBs.

In conclusion, the ER plays a central role in endosymbiosis regulation. Our results demonstrated that LBs originate in specialized domains of the host ER (likely localized near the mesoglea) but disassociate from the ER when migrating and fusing to form large LBs near the coelenteron. Consequently, we predicted that the disruption of host ER homeostasis induced by environmental stress can damage endosymbiotic function

([Oakley et al., 2017](#)). Further research is required to elucidate the precise mechanisms of LB formation, maturation, and catabolism in corals and to examine the roles, apart from energy homeostasis, that LBs might have in coral–Symbiodinaceae endosymbiosis.

## ACKNOWLEDGEMENTS

We thank Yi-Jyun Chen for performing the experiments. We thank Dr. Anderson B. Mayfield and Crystal J. McRae for reviewing the manuscript draft. We thank the anonymous reviewers whose comments/suggestions helped improve and clarify this manuscript.

## ADDITIONAL INFORMATION AND DECLARATIONS

### Funding

This work was supported by a grant from the Ministry of Science and Technology (MOST) of Taiwan (formerly the National Science Council [NSC]; NSC 101-2311-B-291-002-MY3 and MOST 108-2311-B-291-001 to CSC) and by intramural funding from NMMBA (99200311). The funders had no role in study design, data collection and analysis, decision to publish, or preparation of the manuscript.

### Grant Disclosures

The following grant information was disclosed by the authors:

Ministry of Science and Technology (MOST) of Taiwan: NSC 101-2311-B-291-002-MY3, MOST 108-2311-B-291-001.

NMMBA: 99200311.

### Competing Interests

The authors declare there are no competing interests.

### Author Contributions

- Hung-Kai Chen conceived and designed the experiments, performed the experiments, analyzed the data, prepared figures and/or tables, authored or reviewed drafts of the paper, and approved the final draft.
- Sabrina L Rosset analyzed the data, prepared figures and/or tables, and approved the final draft.
- Li-Hsueh Wang performed the experiments, analyzed the data, prepared figures and/or tables, and approved the final draft.
- Chii-Shiarng Chen conceived and designed the experiments, authored or reviewed drafts of the paper, and approved the final draft.

### DNA Deposition

The following information was supplied regarding the deposition of DNA sequences:

The sequences are available at GenBank: [MW659935](#) to [MW659942](#). The reference table and the sequences are available in the [Supplementary File](#).

## Data Availability

The following information was supplied regarding data availability:

The raw images with full-length gels and blots, raw LC-MS/MS data of BiP protein, and transcriptomic sequences of ER stress genes related to LB lipogenesis are available in the [Supplemental Files](#).

## Supplemental Information

Supplemental information for this article can be found online at <http://dx.doi.org/10.7717/peerj.11652#supplemental-information>.

## REFERENCES

- Ariotti N, Murphy S, Hamilton NA, Wu L, Green K, Schieber NL, Li P, Martin S, Parton RG. 2012. Postlipolytic insulin-dependent remodeling of micro lipid droplets in adipocytes. *Molecular Biology of the Cell* 23(10):1826–1837 DOI [10.1091/mbc.e11-10-0847](https://doi.org/10.1091/mbc.e11-10-0847).
- Basseri S, Austin RC. 2012. Endoplasmic reticulum stress and lipid metabolism: mechanisms and therapeutic potential. *Biochemistry Research International* 2012 DOI [10.1155/2012/841362](https://doi.org/10.1155/2012/841362).
- Bertolotti A, Zhang Y, Hendershot LM, Harding HP, Ron D. 2000. Dynamic interaction of BiP and ER stress transducers in the unfolded-protein response. *Nature Cell Biology* 2(6):326–332 DOI [10.1038/35014014](https://doi.org/10.1038/35014014).
- Bolger AM, Lohse M, Usadel B. 2014. Trimmomatic: a flexible trimmer for Illumina sequence data. *Bioinformatics* 30(15):2114–2120 DOI [10.1093/bioinformatics/btu170](https://doi.org/10.1093/bioinformatics/btu170).
- Boström P, Rutberg M, Ericsson J, Holmdahl P, Andersson L, Frohman MA, Borén J, Olofsson S-O. 2005. Cytosolic lipid droplets increase in size by microtubule-dependent complex formation. *Arteriosclerosis, Thrombosis, and Vascular Biology* 25(9):1945–1951 DOI [10.1161/01.ATV.0000179676.41064.d4](https://doi.org/10.1161/01.ATV.0000179676.41064.d4).
- Brasaemle DL, Dolios G, Shapiro L, Wang R. 2004. Proteomic analysis of proteins associated with lipid droplets of basal and lipolytically stimulated 3T3-L1 adipocytes. *Journal of Biological Chemistry* 279(45):46835–46842 DOI [10.1074/jbc.M409340200](https://doi.org/10.1074/jbc.M409340200).
- Chen HK, Wang LH, Chen WNU, Mayfield AB, Levy O, Lin CS, Chen CS. 2017. Coral lipid bodies as the relay center interconnecting diel-dependent lipidomic changes in different cellular compartments. *Scientific Reports* 7(1):1–13 DOI [10.1038/s41598-017-02722-z](https://doi.org/10.1038/s41598-017-02722-z).
- Chen WNU, Kang HJ, Weis V, Mayfield AB, Jiang PL, Fang LS, Chen CS. 2012. Diel rhythmicity of lipid-body formation in a coral-*Symbiodinium* endosymbiosis. *Coral Reefs* 31(2):521–534 DOI [10.1007/s00338-011-0868-6](https://doi.org/10.1007/s00338-011-0868-6).
- Cheng J, Fujita A, Ohsaki Y. 2009. Quantitative electron microscopy shows uniform incorporation of triglycerides into existing lipid droplets. *Histochemistry and Cell Biology* 132:281–291 DOI [10.1007/s00418-009-0615-z](https://doi.org/10.1007/s00418-009-0615-z).
- Chitruj C, Mejhert N, Haas JT, Diaz-Ramirez LG, Grueter CA, Imbriglio JE, Pinto S, Koliwad SK, Walther TC, Farese Jr RV. 2017. Triglyceride synthesis by DGAT1

protects adipocytes from lipid-induced ER stress during lipolysis. *Cell Metabolism* **26**(2):407–418 DOI [10.1016/j.cmet.2017.07.012](https://doi.org/10.1016/j.cmet.2017.07.012).

**Cohen S, Valm AM, Lippincott-Schwartz J.** 2018. Interacting organelles. *Current Opinion in Cell Biology* **53**:84–91 DOI [10.1016/j.ceb.2018.06.003](https://doi.org/10.1016/j.ceb.2018.06.003).

**Crossland C, Barnes D, Borowitzka M.** 1980. Diurnal lipid and mucus production in the staghorn coral *Acropora acuminata*. *Marine Biology* **60**(2–3):81–90 DOI [10.1007/BF00389151](https://doi.org/10.1007/BF00389151).

**Crusoe MR, Alameldin HF, Awad S, Boucher E, Caldwell A, Cartwright R, Charbonneau A, Constantinides B, Edvenson G, Fay S, Fenton J, Fenzl T, Fish J, Garcia-Gutierrez L, Garland P, Gluck J, Gonzalez I, Guermond S, Guo J, Gupta A, Herr JR, Howe A, Hyer A, Härpfer A, Irber L, Kidd R, Lin D, Lippi J, Mansour T, McA'Nulty P, McDonald E, Mizzi J, Murray KD, Nahum JR, Nanlohy K, Nederbragt AJ, Ortiz-Zuazaga H, Ory J, Pell J, Pepe-Ranney C, Russ ZN, Schwarz E, Scott C, Seaman J, Sievert S, Simpson J, Skennerton CT, Spencer J, Srinivasan R, Standage D, Stapleton JA, Steinman SR, Stein J, Taylor B, Trimble W, Wiencko HL, Wright M, Wyss B, Zhang Q, Zyme E, Brown CT.** 2015. The khmer software package: enabling efficient nucleotide sequence analysis. *F1000 Research* **4**:900–900 DOI [10.12688/f1000research.6924.1](https://doi.org/10.12688/f1000research.6924.1).

**Diwu Z, Lu Y, Zhang C, Klaubert DH, Haugland RP.** 1997. Fluorescent molecular probes II. The synthesis, spectral properties and use of fluorescent solvatochromic dapoxyl dyes. *Photochemistry and Photobiology* **66**(4):424–431 DOI [10.1111/j.1751-1097.1997.tb03168.x](https://doi.org/10.1111/j.1751-1097.1997.tb03168.x).

**Federovitch CM, Ron D, Hampton RY.** 2005. The dynamic ER: experimental approaches and current questions. *Current Opinion in Cell Biology* **17**(4):409–414 DOI [10.1016/j.ceb.2005.06.010](https://doi.org/10.1016/j.ceb.2005.06.010).

**Fei W, Wang H, Fu X, Bielby C, Yang H.** 2009. Conditions of endoplasmic reticulum stress stimulate lipid droplet formation in *Saccharomyces cerevisiae*. *Biochemical Journal* **424**(1):61–67 DOI [10.1042/BJ20090785](https://doi.org/10.1042/BJ20090785).

**Fu L, Niu B, Zhu Z, Wu S, Li W.** 2012. CD-HIT: accelerated for clustering the next-generation sequencing data. *Bioinformatics* **28**(23):3150–3152 DOI [10.1093/bioinformatics/bts565](https://doi.org/10.1093/bioinformatics/bts565).

**Gao Q, Goodman JM.** 2015. The lipid droplet—a well-connected organelle. *Frontiers in Cell and Developmental Biology* **3**:49 DOI [10.3389/fcell.2015.00049](https://doi.org/10.3389/fcell.2015.00049).

**Gocze PM, Freeman DA.** 1994. Factors underlying the variability of lipid droplet fluorescence in MA-10 Leydig tumor cells. *Cytometry* **17**(2):151–158 DOI [10.1002/cyto.990170207](https://doi.org/10.1002/cyto.990170207).

**Grabherr MG, Haas BJ, Yassour M, Levin JZ, Thompson DA, Amit I, Adiconis X, Fan L, Raychowdhury R, Zeng Q.** 2011. Full-length transcriptome assembly from RNA-Seq data without a reference genome. *Nature Biotechnology* **29**(7):644–652 DOI [10.1038/nbt.1883](https://doi.org/10.1038/nbt.1883).

- Guo Y, Walther TC, Rao M, Stuurman N, Goshima G, Terayama K, Wong JS, Vale RD, Walter P, Farese RV.** 2008. Functional genomic screen reveals genes involved in lipid-droplet formation and utilization. *Nature* **453**(7195):657–661 DOI [10.1038/nature06928](https://doi.org/10.1038/nature06928).
- Han J, Kaufman RJ.** 2016. The role of ER stress in lipid metabolism and lipotoxicity. *Journal of Lipid Research* **57**(8):1329–1338 DOI [10.1194/jlr.R067595](https://doi.org/10.1194/jlr.R067595).
- Hayes RL, Goreau NI.** 1977. Intracellular crystal-bearing vesicles in the epidermis of scleractinian corals, *Astrangia danae* (Agassiz) and *Porites porites* (Pallas). *The Biological Bulletin* **152**(1):26–40 DOI [10.2307/1540724](https://doi.org/10.2307/1540724).
- Herms A, Bosch M, Reddy BJ, Schieber NL, Fajardo A, Rupérez C, Fernández-Vidal A, Ferguson C, Rentero C, Tebar F.** 2015. AMPK activation promotes lipid droplet dispersion on detyrosinated microtubules to increase mitochondrial fatty acid oxidation. *Nature Communications* **6**(1):1–14 DOI [10.1038/ncomms8176](https://doi.org/10.1038/ncomms8176).
- Jacquier N, Choudhary V, Mari M, Toulmay A, Reggiori F, Schneiter R.** 2011. Lipid droplets are functionally connected to the endoplasmic reticulum in *Saccharomyces cerevisiae*. *Journal of Cell Science* **124**(14):2424–2437 DOI [10.1242/jcs.076836](https://doi.org/10.1242/jcs.076836).
- Langmead B, Salzberg SL.** 2012. Fast gapped-read alignment with Bowtie 2. *Nature Methods* **9**(4):357–359 DOI [10.1038/nmeth.1923](https://doi.org/10.1038/nmeth.1923).
- Lee JS, Mendez R, Heng HH, Yang ZQ, Zhang K.** 2012. Pharmacological ER stress promotes hepatic lipogenesis and lipid droplet formation. *American Journal of Translational Research* **4**(1):102 DOI [10.1194/jlr.R028290](https://doi.org/10.1194/jlr.R028290).
- Levy O, Achituv Y, Yacobi Y, Dubinsky Z, Stambler N.** 2006. Diel ‘tuning’ of coral metabolism: physiological responses to light cues. *Journal of Experimental Biology* **209**(2):273–283 DOI [10.1242/jeb.01983](https://doi.org/10.1242/jeb.01983).
- Levy O, Kaniewska P, Alon S, Eisenberg E, Karako-Lampert S, Bay L, Reef R, Rodriguez-Lanetty M, Miller D, Hoegh-Guldberg O.** 2011. Complex diel cycles of gene expression in coral-algal symbiosis. *Science* **331**(6014):175–175 DOI [10.1126/science.1196419](https://doi.org/10.1126/science.1196419).
- Liu P, Ying Y, Zhao Y, Mundy DI, Zhu M, Anderson RG.** 2004. Chinese hamster ovary K2 cell lipid droplets appear to be metabolic organelles involved in membrane traffic. *Journal of Biological Chemistry* **279**(5):3787–3792 DOI [10.1074/jbc.M311945200](https://doi.org/10.1074/jbc.M311945200).
- Malhotra JD, Kaufman RJ.** 2007. Endoplasmic reticulum stress and oxidative stress: a vicious cycle or a double-edged sword? *Antioxidants & Redox Signaling* **9**(12):2277–2294 DOI [10.1089/ars.2007.1782](https://doi.org/10.1089/ars.2007.1782).
- Mastro R, Hall M.** 1999. Protein delipidation and precipitation by tri-n-butylphosphate, acetone, and methanol treatment for isoelectric focusing and two-dimensional gel electrophoresis. *Analytical Biochemistry* **273**(2):313–315 DOI [10.1006/abio.1999.4224](https://doi.org/10.1006/abio.1999.4224).
- Mishra S, Khaddaj R, Cottier S, Stradalova V, Jacob C, Schneiter R.** 2016. Mature lipid droplets are accessible to ER luminal proteins. *Journal of Cell Science* **129**(20):3803–3815 DOI [10.1242/jcs.189191](https://doi.org/10.1242/jcs.189191).
- Morris JA, Dorner AJ, Edwards CA, Hendershot LM, Kaufman RJ.** 1997. Immunoglobulin binding protein (BiP) function is required to protect cells from endoplasmic

reticulum stress but is not required for the secretion of selective proteins. *Journal of Biological Chemistry* 272(7):4327–4334 DOI 10.1074/jbc.272.7.4327.

- Oakley CA, Durand E, Wilkinson SP, Peng L, Weis VM, Grossman AR, Davy SK. 2017.** Thermal shock induces host proteostasis disruption and endoplasmic reticulum stress in the model symbiotic cnidarian *Aiptasia*. *Journal of Proteome Research* 16(6):2121–2134 DOI 10.1021/acs.jproteome.6b00797.
- Olzmann JA, Carvalho P. 2019.** Dynamics and functions of lipid droplets. *Nature Reviews Molecular Cell Biology* 20(3):137–155 DOI 10.1038/s41580-018-0085-z.
- Peng SE, Chen WNU, Chen HK, Lu CY, Mayfield AB, Fang LS, Chen CS. 2011.** Lipid bodies in coral–dinoflagellate endosymbiosis: proteomic and ultrastructural studies. *Proteomics* 11(17):3540–3555 DOI 10.1002/pmic.201000552.
- Peng SE, Luo YJ, Huang HJ, Lee IT, Hou LS, Chen WNU, Fang LS, Chen CS. 2008.** Isolation of tissue layers in hermatypic corals by N-acetylcysteine: morphological and proteomic examinations. *Coral Reefs* 27(1):133–142 DOI 10.1007/s00338-007-0300-4.
- Ploegh HL. 2007.** A lipid-based model for the creation of an escape hatch from the endoplasmic reticulum. *Nature* 448(7152):435–438 DOI 10.1038/nature06004.
- Pol A, Martin S, Fernandez MA, Ferguson C, Carozzi A, Luetterforst R, Enrich C, Parton RG. 2004.** Dynamic and regulated association of caveolin with lipid bodies: modulation of lipid body motility and function by a dominant negative mutant. *Molecular Biology of the Cell* 15(1):99–110 DOI 10.1091/mbc.e03-06-0368.
- Prattes S, Horl G, Hammer A, Blaschitz A, Graier WF, Sattler W, Zechner R, Steyrer E. 2000.** Intracellular distribution and mobilization of unesterified cholesterol in adipocytes: triglyceride droplets are surrounded by cholesterol-rich ER-like surface layer structures. *Journal of Cell Science* 113(17):2977–2989 DOI 10.1016/S0021-9150(00)81077-1.
- Schneider CA, Rasband WS, Eliceiri KW. 2012.** NIH Image to ImageJ: 25 years of image analysis. *Nature Methods* 9(7):671–675 DOI 10.1038/nmeth.2089.
- To M, Peterson CW, Roberts MA, Counihan JL, Wu TT, Forster MS, Nomura DK, Olzmann JA. 2017.** Lipid disequilibrium disrupts ER proteostasis by impairing ERAD substrate glycan trimming and dislocation. *Molecular Biology of the Cell* 28(2):270–284 DOI 10.1091/mbc.e16-07-0483.
- Trapnell C, Roberts A, Goff L, Pertea G, Kim D, Kelley DR, Pimentel H, Salzberg SL, Rinn JL, Pachter L. 2012.** Differential gene and transcript expression analysis of RNA-seq experiments with TopHat and Cufflinks. *Nature Protocols* 7(3):562–578 DOI 10.1038/nprot.2012.016.
- Vandermeulen J. 1974.** Studies on reef corals. II. Fine structure of planktonic planula larva of *Pocillopora damicornis*, with emphasis on the aboral epidermis. *Marine Biology* 27(3):239–249 DOI 10.1007/BF00391949.
- Volmer R, Ron D. 2015.** Lipid-dependent regulation of the unfolded protein response. *Current Opinion in Cell Biology* 33:67–73 DOI 10.1016/j.ceb.2014.12.002.
- Walter P, Ron D. 2011.** The unfolded protein response: from stress pathway to homeostatic regulation. *Science* 334(6059):1081–1086 DOI 10.1126/science.1209038.

- Wan HC, Melo RC, Jin Z, Dvorak AM, Weller PF.** 2007. Roles and origins of leukocyte lipid bodies: proteomic and ultrastructural studies. *The FASEB Journal* 21(1):167–178 DOI 10.1096/fj.06-6711.
- Welte MA.** 2009. Fat on the move: intracellular motion of lipid droplets. *Biochemical Society Transactions* 37(5):991–996 DOI 10.1042/BST0370991.
- Wilfling F, Haas JT, Walther TC, Farese Jr RV.** 2014. Lipid droplet biogenesis. *Current Opinion in Cell Biology* 29:39–45 DOI 10.1016/j.ceb.2014.03.008.
- Wu H, Carvalho P, Voeltz GK.** 2018. Here, there, and everywhere: The importance of ER membrane contact sites. *Science* 361:6401 DOI 10.1126/science.aan5835.
- Yang H, Galea A, Sytnyk V, Crossley M.** 2012. Controlling the size of lipid droplets: lipid and protein factors. *Current Opinion in Cell Biology* 24(4):509–516 DOI 10.1016/j.ceb.2012.05.012.
- Zehmer JK, Bartz R, Bisel B, Liu P, Seemann J, Anderson RG.** 2009. Targeting sequences of UBXD8 and AAM-B reveal that the ER has a direct role in the emergence and regression of lipid droplets. *Journal of Cell Science* 122(20):3694–3702 DOI 10.1242/jcs.054700.
- Zha BS, Zhou H.** 2012. ER stress and lipid metabolism in adipocytes. *Biochemistry Research International* 2012 DOI 10.1155/2012/312943.
- Zhang S, Wang Y, Cui L, Deng Y, Xu S, Yu J, Cichello S, Serrero G, Ying Y, Liu P.** 2016. Morphologically and functionally distinct lipid droplet subpopulations. *Scientific Reports* 6:29539 DOI 10.1038/srep29539.
- Zhao Y, Tang H, Ye Y.** 2011. RAPSearch2: a fast and memory-efficient protein similarity search tool for next-generation sequencing data. *Bioinformatics* 28(1):125–126 DOI 10.1093/bioinformatics/btr595.
- Zheng Z, Zhang C, Zhang K.** 2010. Role of unfolded protein response in lipogenesis. *World Journal of Hepatology* 2(6):203 DOI 10.4254/wjh.v2.i6.203.